Reaction mechanisms of mixed ionic and electronic conductors used as oxygen electrodes in Solid Oxide Cell: focus on La_1 − xSr_xCo_y − 1Fe_yO_3 − δ and La_2NiO_4 + δ

Lydia Yefsah, Giuseppe Sdanghi, Giuseppe Sassone, Jean-Marc. Bassat, Maxime Hubert, Elisabeth Djurado, Jérôme Laurencin

B1601

Reaction mechanisms of mixed ionic and electronic conductors used as oxygen electrodes in Solid Oxide Cell: focus on $La_{1-x}Sr_xCo_{y-1}Fe_yO_{3-\delta}$ and $La_2NiO_{4+\delta}$

Lydia Yefsah (1,2), Giuseppe Sdanghi (2,3), Giuseppe Sassone (2), Jean-Marc Bassat (3), Maxime Hubert (2), Elisabeth Djurado (1), Jérôme Laurencin (2)

(1) Univ. Grenoble Alpes, CNRS, LEPMI, 38000 Grenoble, France
(2) Univ. Grenoble Alpes, CEA-Liten, DTCH, 38000 Grenoble, France
(3) CNRS, Univ. Bordeaux, ICMCB, 33608 Pessac, France

lydia.yefsah@lepmi.grenoble-inp.fr

Abstract

$La_{1-x}Sr_xCo_{y-1}Fe_yO_{3-\delta}$ (LSCF), a typical oxygen electrode in Solid Oxide Cells (SOCs), is an oxygen-deficient perovskite material. Although this mixed ionic and electronic conductor (MIEC) offers good electrochemical performances, it suffers from chemical decomposition in operation at high temperature. The oxygen over-stoichiometric electrode material $La_2NiO_{4+\delta}$ (LNO) is considered nowadays as an alternative solution to the classical perovskite-based electrodes. Indeed, LNO is chemically stable in a wide range of temperatures and oxygen partial pressures, providing high MIEC conductivity as well as fast oxygen reaction kinetics.

A deep understanding of the reaction mechanisms taking place in a SOC oxygen electrode is a prerequisite before microstructural optimization. In this work, we propose a coupled experimental and modeling approach aimed to investigate the reaction mechanisms for both under- and over-stoichiometric oxygen electrode materials. Two main reaction pathways have been considered, the oxygen incorporation/excorporation at the gas/electrode interface for the bulk path and the direct charge transfer at the Triple Phase Boundary lengths (TPBls) for the surface path. Polarization curves and impedance diagrams under various operating conditions (650-750°C, 0.15 - 1 atm, and ± 100 mA cm^{-2}) have been recorded by using a three-electrode setup. These data were used to calibrate the models based on elementary reactions. In addition, all the microstructural parameters required for the simulation have been computed on a 3D electrode reconstruction obtained by FIB-SEM tomography. A change from the bulk towards the surface path was observed for the LSCF electrode under low anodic polarization, which was explained by the progressive depletion of oxygen vacancies when increasing the anodic polarization. Conversely, a limitation of the bulk path was observed under cathodic polarization for the LNO electrode, which was due to the significant reduction of the oxygen over stoichiometry under these conditions. The impact of the temperature and the pO_2 on the reaction pathways has been also investigated for both materials and is discussed in this article.

Introduction

SOCs are high-temperature electrochemical energy-conversion devices that produce efficiently clean electricity (solid oxide fuel cell, SOFC mode) or hydrogen (solid oxide electrolysis cell, SOEC mode). These technologies are composed of an assembly of two porous electrodes separated by a thin dense electrolyte in Yttria Stabilized Zirconia (YSZ). The porous hydrogen electrode is usually a Nickel and YSZ cermet while mixed ionic and electronic conductors (MIECs) are mostly developed as oxygen electrode materials. This mixed property allows extending the oxygen reaction on the whole gas/electrode interface. The classical MIECs material is the lanthanum doped strontium cobalt ferrite $La_{1-x}Sr_xCo_{y-1}Fe_yO_{3-\delta}$ (LSCF) [1] [2]. This oxygen-deficient perovskite presents a good ionic and electronic conductivity as well as a high oxygen surface exchange rate. However, LSCF suffers from large degradation rates due to chemical decomposition at high operating and reactivity with electrolyte [3] [4] [5]. These degradations induce significant loss in SOCs performances, especially when they are operated in SOEC mode. In this context, rare earth nickelates $Ln_2NiO_{4+\delta}$ (Ln = La, Pr, Nd) are considered nowadays as alternative oxygen electrode materials. The crystal structure of this over-stoichiometric material consists of $LnNiO_3$ perovskite block inter-grown between LnO rock-salt layers. The excess oxygen occupies interstitial sites within the LnO layers. Among the different components, $La_2NiO_{4+\delta}$ (LNO) has been chosen in this study thanks to its chemical stability in a wide range of temperature [6]. This work aims to analyze, by an experimental and a modeling approach, the effect of the temperature, polarization, and oxygen partial pressure on the reaction pathways for LSCF and LNO electrodes.

1. Scientific Approach

1.1 Experiments

The two electrode materials, LSCF and LNO, were deposited by screen-printing on each side of a circular and dense 8YSZ electrolyte (thickness = 260 µm, diameter = 25 mm). To prevent the reactivity with YSZ that leads to the formation of insulating phases [7] [8], a $Ce_{0.8}Gd_{0.2}O_{2-\delta}$ (CGO) barrier layer of 2 µm of thickness was added in between the electrodes, and the electrolyte. The symmetrical cells were then tested in a 3-electrodes setup. A platinum wire was positioned at the periphery of the electrolyte membrane and used as a reference electrode (RE). Two platinum grids with a mesh of 3600 meshes.cm^{-2} and a surface equal to the electrodes were used as current collectors. It can be noticed that a thick disk in porous gold was also added between the ceramic housing and the platinum grids so that each electrode surface can be considered equipotential. A load of 0.7 kg/cm² was applied to ensure the electric contact between the metallic grids and the electrodes. At the beginning of the test, the cells were heated up to 800°C at a rate of 1°C/min. This temperature has been maintained during several hours until the stabilization of the electrochemical impedance spectra (EIS) measured at open circuit potential (OCP).

Electrochemical characterizations were then carried out at a temperature of 750, 700 and 650°C under air condition, with a gas flow rate of ≈ 2NL.min^{-1}. For each temperature, polarization curves have been recorded for both cells whereas EIS diagrams were acquired at OCP, in a frequency range of 10^6 to 10^{-2} Hz, with an amplitude of ± 10 mA/cm^{-2}. For the temperature of 700°C, the electrochemical characterizations were complemented by EIS

diagrams measured under anodic and cathodic current (with $i_{dc} = \pm$ 50 mA/cm² for LSCF electrode and $i_{dc} = \pm$ 100 mA.cm² for LNO electrode) and over a large range of oxygen partial pressure from 0.1 to 1 atm.

2.2 Model Description

An elementary model framework for MIEC electrodes has been developed and used to investigate the LSCF and LNO reaction mechanisms occurring under anodic and cathodic polarization. In this approach, surface and bulk species are taken into account as well as their transport in the electrodes phases. A temporal term is also added to each mass/charge balance for the EIS computations. The mass transfer in the LNO and LSCF is calculated through the chemical diffusivity of the oxygen interstitials or vacancies, respectively, while the electronic current density is modeled using a classical Ohm's law. Both molecular and Knudsen diffusions are taken into account for the mass transport in the gas phase. Finally, the diffusion of oxygen adatoms O_{ads}, oxygen ions O^{-}_{ads} and molecular oxygen $O_{2\,ads}$ at the surface of both materials is computed using a classical Fick's law.
The proposed model considers two possible reaction pathways for oxygen oxidation/reduction divided into a sequence of elementary steps as represented in Figure 1 in the electrolysis mode. The "bulk path" is characterized by an ionic transfer at the electrode/electrolyte interface (R1). After diffusion of the oxygen interstitials (for LNO) or oxygen vacancies (for LSCF) in the bulk of the electrode material, the oxygen is ex-corporated to produce oxygen adatoms on the electrode surface (R2). In parallel, the "surface path" considers direct oxidation at the TPBls (R3) leading to the formation of oxygen ions on the electrode surface. Then, in both cases, the second reaction of charge transfer (R4) takes place on the surface to produce oxygen adatoms that can be associated (R5) and desorbed (R6) in the porosity of the electrodes.

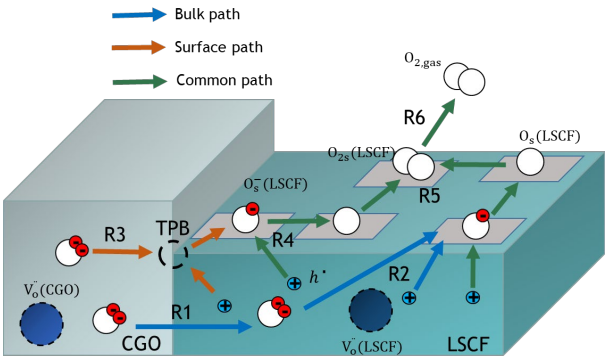

Figure 1 - Schematic description of the reaction pathway considered in the elementary model (in electrolysis mode) represented for the LSCF electrode.

The kinetic constants have been estimated by calibrating the model on the LSCF and LNO polarization curves. Due to the influence of the microstructure on the electrochemical response, all the microstructural properties used as inputs in the model have been extracted from 3D reconstructions obtained for both electrodes. Thereafter, the model has been validated using the electrochemical impedance diagrams recorded at OCP and under polarization for different oxygen partial pressures. The elementary kinetic model has been already published for the LSCF electrode [9] while the one for the LNO is an adaptation of a simplified version available in [10].

2. Experimental Results

The experimental electrode polarization curves η-i at 650°C, 700°C, and 750°C are represented in Figure 2 for the LSCF and LNO oxygen electrodes.
As expected, it can be noticed that the electrode performances are thermally activated [11] [12]. To the OCP, a non-symmetrical shape of the η-i curves is observed at 650°C and 700°C for both electrodes. However, it is worth mentioning that the electrode performances are better under anodic polarization (SOEC mode) for the LNO electrode, whereas the LSCF electrode exhibits lower overpotentials under cathodic current (SOFC mode). Within the narrow investigated overpotential range, a linear behavior of the η-i curves is observed at 750°C. The dissymmetry of the polarization curves at a lower temperature can be explained either by a change in the reaction mechanism or the rate-determining steps. Conversely, a unique dominant mechanism with the same co-limitations could explain the linearity of η-i curves at 750°C in the studied conditions.

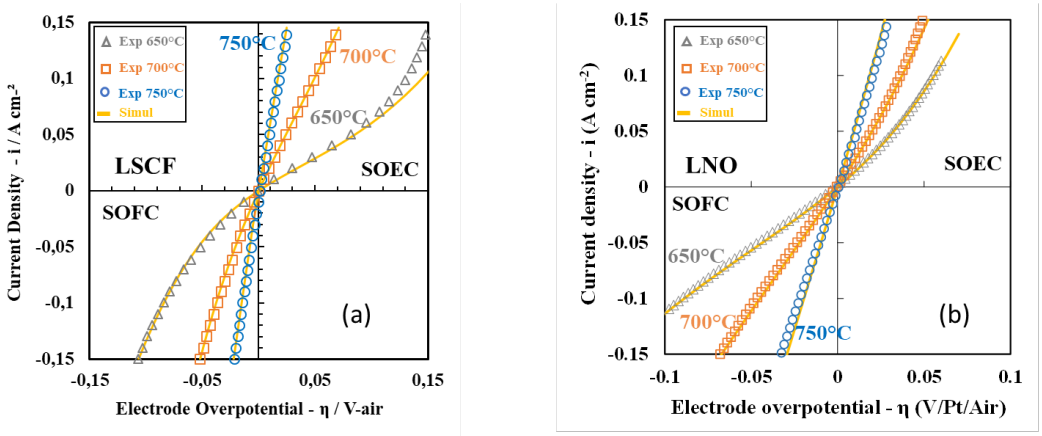

Figure 2 - Experimental (marks) and simulated (solid lines) polarization curves obtained at 650, 700, and 750 °C under air for a) LSCF and b) LNO electrodes.

The EIS diagrams acquired at OCP under air at 650 °C, 700 °C, and 750 °C are shown in Figure 3 for the LNO and LSCF materials. It is worth noting that the absolute values of the polarization resistances cannot be directly compared between the two electrodes since they present rather different microstructures due to the fabrication. Nevertheless, the shape of the impedance spectra can give key information about the reaction mechanisms. Indeed, for the LSCF electrode, the impedance spectra show a "Gerischer-type" element, whatever the temperature. A small contribution can be noticed at low frequencies on the EIS diagram at 750°C which can be attributed to a limitation in the gas conversion reaction [13]. On the contrary, the EIS diagrams at OCP of the LNO electrode show a different evolution depending on the temperature. A “Gerisher-type” element is observed at 650°C whereas the diagrams present a more depressed semi-circle at 700°C and 750°C. This evolution suggests an influence of the temperature on the reaction mechanism at OCP for the LNO electrode. On the other hand, the non-evolution of the shape of the EIS diagrams for the LSCF electrode may suggest the presence of a unique dominant reaction mechanism in the range of the studied temperature.

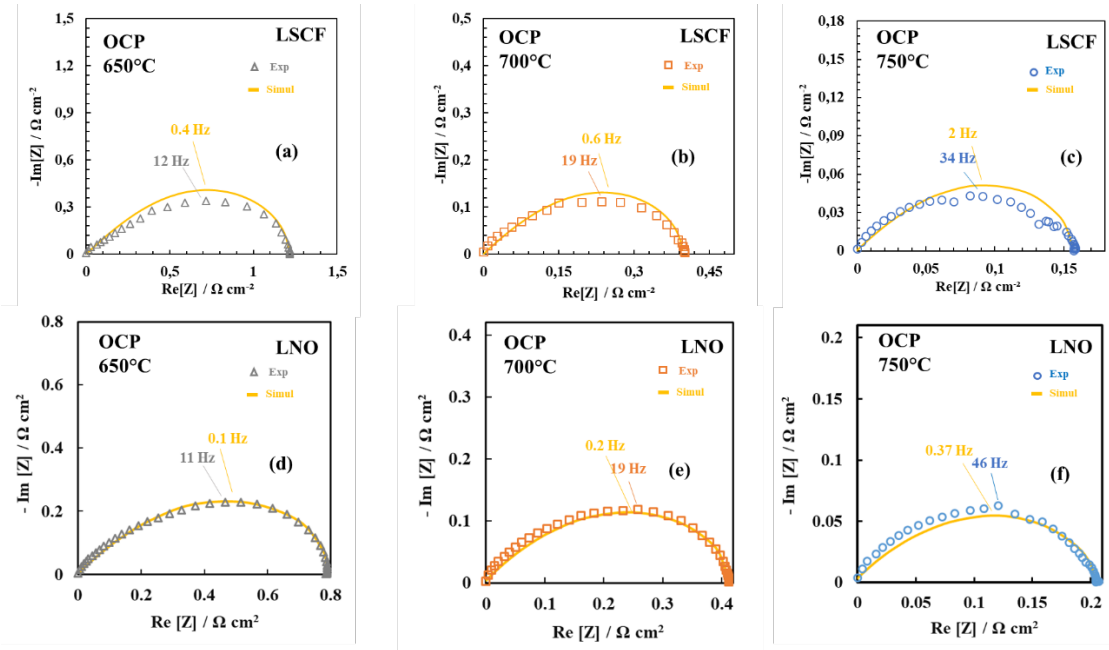

Figure 3 - Experimental (marks) and simulated (solid lines) EIS diagrams under air at 650 °C, 700 °C, and 750 °C for LSCF (a, b, c) and LNO (c, d, f) electrodes

For both cases, the EIS diagrams recorded under dc current density at 700°C have not revealed a change in the shape of the impedance spectra [9] [10] compared to the OCP. These results suggest that, for both electrodes, there is no change in the reaction mechanism at 700°C under polarization for the limited investigated range of dc current. The evolution of the impedance spectroscopy with the oxygen partial pressure is shown in Figure 4. As expected, the polarization resistance of both electrodes decreases with increasing pO_2.

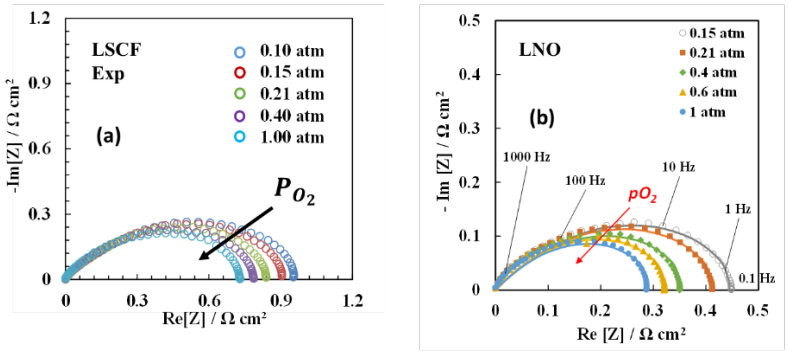

Figure 4 - Impedance diagrams (Nyquist plots) recorded at 700°C for the investigated range of oxygen partial pressure for a) LSCF and b) LNO electrodes.

3. Modeling Results and Discussion

3.1 Model calibration and validation

The missing parameters for the models (i.e. the forward kinetic constants for all the reactions, the surface diffusion coefficients, and surface coverages at equilibrium for pO_2=0.21 atm [9] [10]) have been obtained by adjusting the simulations on the experimental polarization curves. The results of this fitting procedure are given in Fig. 2 for the two

electrodes. Once the model was calibrated, the validation was carried out by simulating the impedance spectra without additional fitting. As shown in Fig. 3, the model for LSCF or LNO electrode can simulate accurately the impedance diagrams at OCP for the three investigated temperatures. Moreover, the reaction order *n* was deduced from the experimental and simulated impedance spectra (Fig. 4) according to :

$$R_{pol} \propto (pO_2)^{-n} \quad (1)$$

These simulated reaction orders are in good agreement with the experimental ones. Indeed, the errors between the computed and experimental coefficients do not exceed 12% for LSCF and only 9% for LNO. Therefore, the model for the two electrodes can be considered validated.

3.2 Effect of polarization, temperature, and pO_2 on the reaction pathways

Thanks to the model, the electrode reaction mechanism can be studied as a function of the temperature, polarization, and oxygen partial pressure. For this purpose, the parameter ξ is introduced to quantify the relative contribution of the surface or bulk path in the electrode operation. It is expressed as the kinetic rate ratio between (i) the oxygen ad-ions produced at the TPBls for the surface path and (ii) the oxygen ad-ions produced by excorporation all along with the electrode thickness for the bulk path:

$$\xi = v_3 \Big/ \int_{z=0}^{z=\ell} v_2 \, dz \quad (1)$$

where v_3 and v_2 are kinetic rates for the charge transfer reactions R3 and R2, respectively. The term ℓ represents the electrode thickness. According to this definition, the reaction mechanism is dominated by the “bulk path” when the ratio is lower than one $(\xi < 1)$. On the opposite, a value higher than one $(\xi > 1)$ indicates a mechanism controlled by the “surface path”.

For the LSCF electrode, Figure 5a shows an increase of the ratio ξ when increasing the anodic polarization. A transition from the bulk path $(\xi < 1)$ to the surface path $(\xi > 1)$ is thus observed at low anodic current density for the three temperatures. This behavior can be explained by the evolution of the kinetics rates plotted in Figure 5b as a function of the current density. Indeed, when the anodic polarization increases, the oxygen excorporation rate becomes bounded while the direct oxidation at TPBs remains activated. This behavior is related to the strong decrease of the oxygen vacancies concentration in the LSCF when increasing the anodic polarization [14] [15]. In other words, the under-stoichiometry δ falls to zero under anodic polarization in such a way that the material can no longer accept oxygen [16]. In parallel, the surface concentrations of the adsorbed species involved in the surface path are increased and remain unlimited (since the sum of surface coverages of all the adsorbates remains lower than the coverage of the available sites). On the other hand, the opposite trend is observed under cathodic polarization. In this case, the incorporation reaction is activated because the concentration of vacancies is increased when increasing the cathodic polarization without limitation (indeed, δ remains lower than δ^{max}). Conversely, the charge transfer at TPBs becomes limited since the surface coverages decreases down to zero.

The same behavior is obtained for the three investigated temperatures (Figure 5a). Nevertheless, the influence of temperature on the reaction mechanism is not negligible. Indeed, the contribution of the surface path becomes rapidly more important at 650°C (Figure 5a). At intermediate temperatures (700°C and 750°C), the slopes of the curves are

less steep. These results explain the strong dissymmetry of the experimental polarization curves at 650°C while a more linear behavior is observed at 750°C. To summarize, for the LSCF oxygen electrode, the bulk path appears as the dominant pathway under fuel cell conditions regardless of the temperature. For electrolysis mode, a transition from the bulk path to the surface path appears when the anodic polarization is increased. This transition occurs when the oxygen vacancy concentration tends to zero.

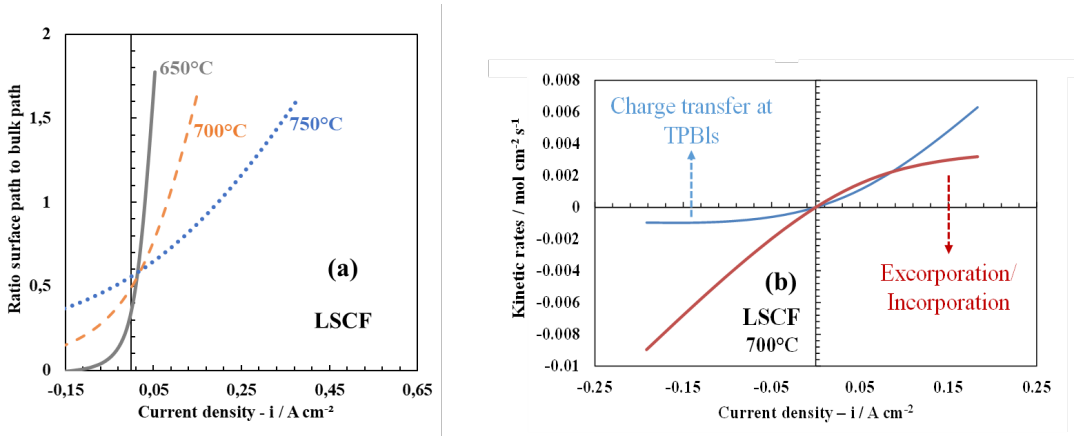

Figure 5 – (a) Ratio of the surface to the bulk path as a function of the current density plotted for the LSCF electrode at 650°C, 700°C, 750°C, and 800°C. (b) Kinetics rates for the charge transfer at TPBs and the oxygen excorporation/incorporation reaction (integrated along with the electrode thickness) as a function of the current density at 700°C, for the LSCF electrode.

The same analysis has been conducted on the over-stoichiometric LNO which exhibits an opposite behavior compared to the LSCF. Indeed, as shown in Figure 6a, the surface-to-bulk path ratio decreases with increasing the overpotentials from cathodic to anodic polarization. This behavior can also be explained by the kinetics rates of the charge transfer at TPBIs and the oxygen excorporation/incorporation reaction (integrated along with the electrode thickness) plotted as a function of the electrode overpotential (Figure 6b). Indeed, under cathodic polarization, the charge transfer at TPBIs remains strongly activated while the oxygen incorporation reaction becomes bounded. This behavior, which is responsible for the limitation of the bulk path, is directly linked to the concentration of oxygen interstitial in the LNO. Indeed, the simulations have revealed that the concentration of oxygen interstitial becomes very low under cathodic polarization. According to Fig. 6b, the surface path is thus predominant under the investigated range of the cathodic currents. Nevertheless, the charge transfer at TPBIs should also tend towards a limitation when the surface coverage at the LNO surface falls to zero. However, it seems that this limitation is not reached even for the higher cathodic polarization achieved in this work.

Under anodic polarization, both surface and bulk paths remain activated (Fig. 6b). Indeed, the concentration of oxygen interstitial is increased with increasing the polarization without reaching the maximum value of oxygen over-stoichiometry (i.e. δ remains much lower than $\delta_{max} = 0.15$ for LNO [17]). On the other hand, the direct oxidation at TPBs is still promoted since the adsorption sites are not saturated under the applied anodic polarization. These observations allow explain the results obtained on the experimental electrode polarization curves η-i (Figure 2b). Indeed, the higher performances of the LNO electrode under anodic polarization are explained by the contribution of both bulk and surface paths to the reaction mechanism while only the surface path remains activated under cathodic polarization.

The impact of the temperature on the ratio is shown in Figure 6a. At OCP, the bulk path at 650°C controls the reaction mechanism ($\xi < 1$) while the surface path becomes predominant at higher temperature ($\xi > 1$). Thus, it can be stated that the temperature promotes the contribution of the charge transfer at the TPBls for the LNO electrode.

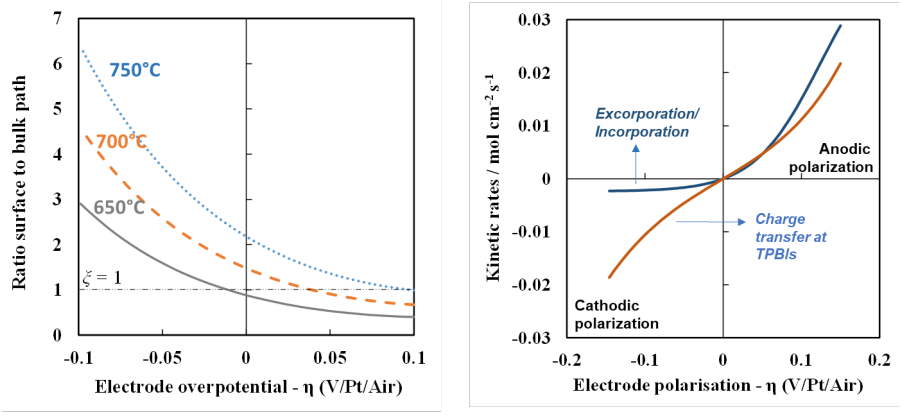

Figure 6 – (a) Ratio of the surface to the bulk path as a function of the current density plotted for the LNO electrode at 650°C, 700°C, and 750°C. (b) Kinetics rates for the charge transfer at TPBs and the oxygen excorporation/incorporation reaction (integrated along with the electrode thickness) as a function of the current density at 700°C, for the LNO electrode. (c) Oxygen over stoichiometry in the electrode thickness, under air, at 700°C, at different polarization.

Simulations have also been carried out by changing the oxygen partial pressure from 0.10 atm to 1 atm (Figure 7). Whatever the current density, it has been found that the ratio increases with increasing pO_2 for the LSCF electrode. This statement is explained because the under-stoichiometry is reduced at high oxygen partial pressure [16]. The opposite behavior has been obtained for the LNO electrode. Indeed, the concentration of interstitials increases with the oxygen partial pressure.

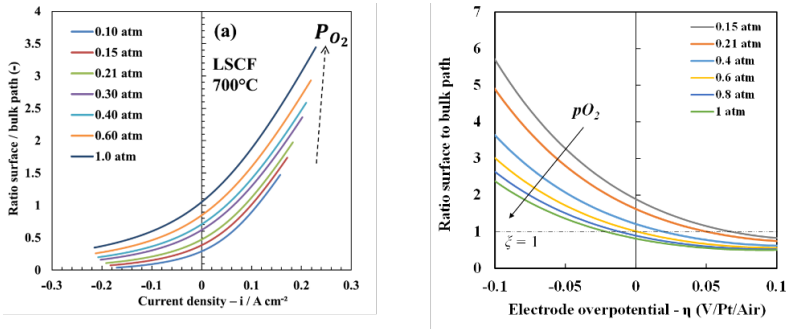

Figure 7 - Ratio of the surface to the bulk path as a function of the electrode overpotential at OCP and 700°C for different oxygen partial pressure for (a) LSCF and (b) LNO.

From this analysis, it appears that the LNO over-stoichiometric material is especially well adapted for an operation in the electrolysis mode. Indeed, it has been shown that both surface and bulk paths are promoted under anodic polarization. This result is consistent with the higher performances obtained for the material when operated in SOEC mode. Regarding the oxygen-deficient LSCF material, it has been found that the bulk path is predominant for cathodic polarization whereas the surface path becomes favored under anodic current.

These statements mean that the material can be operated in both modes. However, its performances are slightly higher in fuel cell mode. To enhance the surface path and thus increase the electrode efficiency, it has been shown that a composite electrode made of LSCF/CGO is a relevant solution [18]. The precise role of CGO in an LNO/CGO composite electrode on its operation and performances still needs to be studied. Moreover, the stability of these electrodes for long-term operations remains also a subject of investigation for the two materials.

Conclusion

Elementary models have been developed and used to predict the electrochemical response of the classical oxygen-deficient oxide $La_{1-x}Sr_xCo_{y-1}Fe_yO_{3-\delta}$ (LSCF) and the alternative oxygen over-stoichiometric material $La_2NiO_{4+\delta}$ (LNO). To validate the models, dedicated experiments have been performed on symmetrical cells using a three-electrode configuration. For the two materials, the determination of the unknown parameters of the models has been done by fitting the experimental electrode polarization curves at three temperatures (650°C, 700°C, and 750°C). For the validation, the impedance spectra at OCP and under polarization for different oxygen partial pressures have been computed without additional fitting. A good agreement between the experimental and the simulations has been obtained.

Once validated, the models have been used to analyze the electrochemical response of the LSCF and LNO materials by investigating the reaction mechanisms as a function of the polarization. For the LSCF, the 'bulk' path related to the oxygen exchange with the material appears as the dominant pathway under cathodic current regardless of the temperature. However, the 'surface' path associated with the charge transfer at TPBls is activated under anodic polarization. This behavior has been ascribed to the strong decrease of the oxygen vacancies concentration in the LSCF when increasing the anodic polarization.
For the LNO electrode, it has been found that both the 'bulk' and 'surface' path are favored under anodic current while only the 'surface' path remains active under cathodic polarization. In this case, the limitation of the 'bulk' path is due to the decrease of the oxygen interstitial concentration in the LNO lattice. These results have allowed explain the better performances obtained for this material in SOEC mode.

References

[1] N. H. Menzler, D. Sebold, and O. Guillon, "Post-test characterization of a solid oxide fuel cell stack operated for more than 30,000 hours: The cell," *Journal of Power Sources*, vol. 374, pp. 69–76, Jan. 2018, doi: 10.1016/j.jpowsour.2017.11.025.

[2] C. Endler-Schuck, A. Leonide, A. Weber, S. Uhlenbruck, F. Tietz, and E. Ivers-Tiffée, "Performance analysis of mixed ionic–electronic conducting cathodes in anode supported cells," *Journal of Power Sources*, vol. 196, no. 17, pp. 7257–7262, Sep. 2011, doi: 10.1016/j.jpowsour.2010.11.079.

[3] Z. Pan, Q. Liu, L. Zhang, X. Zhang, and S. H. Chan, "Effect of Sr Surface Segregation of La0.6Sr0.4Co0.2Fe0.8O3 − δ Electrode on Its Electrochemical Performance in SOC - IOPscience." https://iopscience.iop.org/article/10.1149/2.0371512jes (accessed May 02, 2022).

[4] F. Tietz, A. Mai, and D. Stöver, "From powder properties to fuel cell performance – A holistic approach for SOFC cathode development," *Solid State Ionics*, vol. 179, no. 27, pp. 1509–1515, Sep. 2008, doi: 10.1016/j.ssi.2007.11.037.

[5] S. Uhlenbruck, T. Moskalewicz, N. Jordan, H.-J. Penkalla, and H. P. Buchkremer, "Element interdiffusion at electrolyte–cathode interfaces in ceramic high-temperature fuel cells," *Solid State Ionics*, vol. 180, no. 4, pp. 418–423, Apr. 2009, doi: 10.1016/j.ssi.2009.01.014.
[6] V. Vibhu, J.-M. Bassat, A. Flura, C. Nicollet, J.-C. Grenier, and A. Rougier, "Influence of La/Pr ratio on the ageing properties of La2-xPrxNiO4+ δ as cathodes in IT-SOFCs," *ECS Transactions*, vol. 68, no. 1, p. 825, 2015.
[7] M. D. Anderson, J. W. Stevenson, and S. P. Simner, "Reactivity of lanthanide ferrite SOFC cathodes with YSZ electrolyte," *Journal of Power Sources*, vol. 129, no. 2, pp. 188–192, Apr. 2004, doi: 10.1016/j.jpowsour.2003.11.039.
[8] A. Montenegro-Hernández *et al.*, "Reactivity at the Ln2NiO4+δ/electrolyte interface (Ln = La, Nd) studied by Electrochemical Impedance Spectroscopy and Transmission Electron Microscopy," *Journal of Power Sources*, vol. 265, pp. 6–13, Nov. 2014, doi: 10.1016/j.jpowsour.2014.04.082.
[9] E. Effori *et al.*, "An Elementary Kinetic Model for the LSCF and LSCF-CGO Electrodes of Solid Oxide Cells: Impact of Operating Conditions and Degradation on the Electrode Response," *J. Electrochem. Soc.*, vol. 168, no. 4, p. 044520, Apr. 2021, doi: 10.1149/1945-7111/abf40a.
[10] G. Sdanghi *et al.*, "Reaction Mechanisms of La $_2$ NiO $_{4+\delta}$ Oxygen Electrodes Operated in Electrolysis and Fuel Cell Mode," *J. Electrochem. Soc.*, vol. 169, no. 3, p. 034518, Mar. 2022, doi: 10.1149/1945-7111/ac58c3.
[11] X. Tong, F. Zhou, S. Yang, S. Zhong, M. Wei, and Y. Liu, "Performance and stability of Ruddlesden-Popper La2NiO4+δ oxygen electrodes under solid oxide electrolysis cell operation conditions," *Ceramics International*, vol. 43, no. 14, pp. 10927–10933, Oct. 2017, doi: 10.1016/j.ceramint.2017.05.130.
[12] F. Monaco *et al.*, "Experimental validation of a La0.6Sr0.4Co0.2Fe0.8O3-δ electrode model operated in electrolysis mode: Understanding the reaction pathway under anodic polarization," *Solid State Ionics*, vol. 319, pp. 234–246, Jun. 2018, doi: 10.1016/j.ssi.2018.02.012.
[13] J. Nielsen, T. Jacobsen, and M. Wandel, "Impedance of porous IT-SOFC LSCF:CGO composite cathodes," *Electrochimica Acta*, vol. 56, no. 23, pp. 7963–7974, Sep. 2011, doi: 10.1016/j.electacta.2011.05.042.
[14] J. Laurencin *et al.*, "Reactive Mechanisms of LSCF Single-Phase and LSCF-CGO Composite Electrodes Operated in Anodic and Cathodic Polarisations," *Electrochimica Acta*, vol. 174, pp. 1299–1316, Aug. 2015, doi: 10.1016/j.electacta.2015.06.080.
[15] M. Hubert *et al.*, "Role of microstructure on electrode operating mechanisms for mixed ionic electronic conductors: From synchrotron-based 3D reconstruction to electrochemical modeling," *Solid State Ionics*, vol. 294, pp. 90–107, Oct. 2016, doi: 10.1016/j.ssi.2016.07.001.
[16] S. R. Bishop, K. L. Duncan, and E. D. Wachsman, "Surface and Bulk Defect Equilibria in Strontium-Doped Lanthanum Cobalt Iron Oxide," *J. Electrochem. Soc.*, vol. 156, no. 10, p. B1242, 2009, doi: 10.1149/1.3194783.
[17] T. Nakamura, R. Oike, Y. Ling, Y. Tamenori, and K. Amezawa, "The determining factor for interstitial oxygen formation in Ruddlesden–Popper type La 2 NiO 4 -based oxides," *Physical Chemistry Chemical Physics*, vol. 18, no. 3, pp. 1564–1569, 2016, doi: 10.1039/C5CP05993C.
[18] E. Effori *et al.*, "Reaction Mechanism and Impact of Microstructure on Performances for the LSCF-CGO Composite Electrode in Solid Oxide Cells," *Fuel Cells*, vol. 19, no. 4, pp. 429–444, 2019, doi: 10.1002/fuce.201800185.

Keywords: SOFC, SOEC, MIECs, $La_{1-x}Sr_xCo_{y-1}Fe_yO_{3-\delta}$ (LSCF), $La_2NiO_{4+\delta}$ (LNO), reaction mechanisms.